Electro-active elastomer composite based on doped titanium dioxide Electro-active elastomer composite based on doped titanium dioxide

Alaedine Kossi, Georges Bossis, Jacques Persello

▶ To cite this version:

Electro-active elastomer composite based on doped titanium dioxide

Alaedine Kossi[*], Georges Bossis and Jacques Persello

Laboratoire de Physique de la Matière Condensée LPMC, CNRS UMR 7336, University of Nice-Sophia

Antipolis, Parc Valrose 06108 Nice, France

*Corresponding author: Alaedine Kossi; Tel: +33 492 076 535; E-mail: alaedine.kossi@gmail.com

Electro-active elastomer composite based on doped titanium dioxide

Alaedine Kossi[*], Georges Bossis and Jacques Persello

Laboratoire de Physique de la Matière Condensée LPMC, CNRS UMR 7336, University of Nice-Sophia

Antipolis, Parc Valrose 06108 Nice, France

[*]Corresponding author: Alaedine Kossi; Tel: +33 492 076 535; E-mail: alaedine.kossi@gmail.com

Abstract: Recently, electro-active composites have been considered by several researchers because they exhibit an interesting change in their viscoelastic properties under an applied electric field. However, their relative elastic modulus change $\Delta G'=G'(E)-G'(0)$ is still low and rarely exceed 100 kPa. In this article, we demonstrated that, by synthesizing mesoporous aggregates of titanium dioxide (TiO_2) and by adsorbing acetylacetone dipolar molecule (Acac) onto the TiO_2 surface, the TiO_2-Acac/PDMS electrorheological elastomer achieved a relative elastic modulus change $\Delta G'$ higher than 500 kPa for an applied electric field of 2 kV mm^{-1}. The dependence of the electrorheological response of TiO_2-Acac/PDMS on the DC electric field strength, AC electric field frequency and shear strain magnitude was discussed regarding the conductivity ratio and permittivity ratio between doped TiO_2 semiconducting particles and the PDMS matrix. The high electrorheological performance of TiO_2-doped Acac as semiconducting particles filled in the elastomeric matrix makes this kind of material a promising candidate for application in the automotive industry, robotics, vibration isolators, building applications or electro-active actuators.

Keywords: electrorheological elastomer, electromechanical properties, semiconductor-insulator composites, TiO_2 colloidal particles, PDMS cross-linked matrix

1. Introduction

Magnetorheological and electrorheological fluids are suspensions of micro- or sub-microparticles dispersed in a liquid matrix whose viscosity can be changed by the application of a magnetic or an electric field, respectively. Their solid counterparts are magnetorheological elastomers (MREs) and electrorheological elastomers (EREs).

Magnetorheological elastomers can exhibit a change of their Young's modulus of several hundred kPa under the application of a magnetic field of 0.2-0.5 Tesla and have numerous applications as actuators, vibration isolators or variable capacitors.[1, 2]

Electrorheological elastomers (EREs) are made by suspending semiconducting particles in a cross-linkable insulating polymer. The semiconducting particles are aligned under an applied electric field to form columns in the insulating medium and then the structured dispersion is cross-linked to maintain the anisotropic structure in the polymeric network. In response to an applied electric field ERE composites manifest a rapid and reversible change of modulus. The main cause inducing the ER effect is the mismatch in dielectric constant and conductivity between semiconducting particles and insulating medium that generate dipolar interactions in the presence of an AC or DC electric field. Theoretical models based on linear electrostatics have been developed to understand the physical mechanisms involved in the ER effect, regarding the role of the permittivity and conductivity in the interaction forces between particles. These studies showed that the attraction force in ER fluids increases with the applied electric field according to a quadratic law $F_{elec} \propto E_0^2$.[3-5] However, lower exponents ($1 \leq n < 2$) in the dependence of F_{elec} on E_0 were observed experimentally at a high applied electric field.[6,7] This deviation from the quadratic law was interpreted theoretically by considering, in addition to the solid particle conductivity, the dependence of the matrix conductivity on the electric field which gives rise to a saturation of the local electric field.[8,-16]

The possibility to vary the electromechanical characteristics of EREs and their structural stability make them attractive for developing new smart materials with potential application in the automotive industry, robotics and prosthetic limbs, vibration isolators, building applications and electro-active actuators. [17-25] For this purpose, ERE composites containing different inclusions and dispersed in different matrices, PANI/PDMS,[22] PbTiO$_3$/AR7,[26] Starch/Silicone oil/Silicone rubber,[27,] [28] polythiophene/polyisoprene,[29] Pb(Zr$_{0.5}$,Ti$_{0.5}$)O$_3$/Acrylic rubber,[30] polydiphenylamine/poly(styrene-block-isoprene-block-

styrene,[31] poly(p-phenylene)/Acrylic elastomer,[32] or cellulose/BMIMCl gel,[33] have been investigated. These systems exhibited an increase of their electromechanical properties, and, in particular, of their storage modulus sensitivity $\{(G'(E)-G'(0))/G'(0)\}$. However their relative modulus change $\{G'(E)-G'(0)\}$ was still low and rarely exceeded 100 kPa (compared for instance to 1 MPa for the magnetorheological elastomers (MREs)). Furthermore the matrices used for these EREs were too soft (zero field modulus around 100 kPa: cf. table 2) for most of the applications. Other type of ER materials based on a particular morphology of semiconducting particles emerged and showed an interesting ER effect when used as electrorheological fluids (ERFs).[34-37] It has been reported that the use of mesoporous Ce-doped TiO_2 enhanced the ER response of Ce-doped TiO_2/silicone oil ER fluid and its yield stress was 20 times higher than that of pure dense TiO_2/PDMS fluid.[38, 39] Other workers reported that ERFs based on nano-sized particles showed a so called giant electrorheological effect (GER) when the nanoparticles were coated by molecules having high dipole moments.[40, 41]

In this work, we investigated the response of an electrorheological elastomer (ERE) based on doped titanium dioxide. The specificity of this material lies in three main points: (i) the modification of the intrinsic properties of pure TiO_2 by adding an aluminium cation (Al^{3+}) as substitution impurities of (Ti^{4+}) in the TiO_2 lattices during their growth, (ii) the synthesis of TiO_2 aggregated nanoparticle with a high specific surface area and (iii) the adsorption of Acetylacetone dipolar molecules (Acac) as a doping agent on the TiO_2 surface. The aim underlying these choices was the improvement of relative modulus change ($\Delta G'$) developed by conventional electrorheological elastomers. Indeed, by proceeding so, it was expected that the dielectric properties of the semiconducting particles were improved, the attraction force between particles (when subjected to an external electric field) was amplified, and therefore the electro-rheological response was enhanced. In a previous study we have shown that by doping TiO_2 nanoparticles with Acac we could obtain a good ER fluid with a large increase of

shear modulus.[42] The aim of this work was to obtain such a high field induced modulation, not in the fluid phase but in an elastomeric matrix having a zero field modulus high enough, like PDMS, to be used for active damping applications. This result is not at all granted because the cross-linking pre-polymers are about one hundred times more viscous than the silicone oil used for ER fluid and also because the chain like structure induced by the field can be partly destroyed by the cross-linking process. Here we investigated the electrorheological response of 20 v. % Acac-doped TiO_2 semiconducting particles that were embedded and aligned in PDMS cross-linkable matrix as an ERE. In the first section we present the process used for synthesizing the TiO_2 particles, their morphological characterization, then the preparation of the TiO_2-Acac/PDMS ERE and the experimental conditions for measuring the shear moduli (elastic modulus G' and loss modulus G"). In the second section we first study the kinetics of polymerization by following the viscoelastic properties of samples under an oscillatory shear with and without field during curing. Then we present the electrorheological response of the cross-linked material in terms of the shear modulus increase and of induced current versus electric field amplitude and frequency; here the obtained results were discussed qualitatively in relation to the non linear model of conductivity. Finally we demonstrate the variation in the viscoelastic properties of the TiO_2-Acac/PDMS ERE versus the magnitude of the shear strain, for an AC and DC applied electric field.

2. Experimental section

2-a Particles synthesis

Nano-sized TiO_2 powder was synthesized via a sol–gel method,[42] using titanium tetraisopropoxide (Sigma-Aldrich, 98 %, solution), 2-Propanol (Sigma-Aldrich, ACS reagent, ≥99.5 %), aluminium isopropoxide (Aldrich, 99.99 %), ammonium hydroxide (Sigma-Aldrich, 28 % NH_3 in H_2O), acetylacetone (Sigma-Aldrich, ReagentPlus®, ≥99 %), nitric acid (Sigma-Aldrich, ACS reagent, 70 %), acetic acid (Sigma-Aldrich, ACS reagent, ≥99.7 %) and ultrapure water (≥18 MΩ.cm) as starting materials. In a typical procedure, titanium (IV)

tetraisopropoxide (0.388 mol), was rapidly added to ultrapure water (640 ml) and then stirred for 30 min. A white precipitate formed immediately upon addition of the titanium (IV) isopropoxide. The resultant colloid was recovered by centrifugation (10000 g for 30 min). The centrifugation cake was added into a jacketed three-necked flask reactor equipped with a mechanical stirring containing 750 ml of an aqueous solution, of molar composition ; 0.36 M nitric acid, 1 M acetic acid and 0.05 M aluminium isopropoxide. Al^{3+} was used here in small quantity as impurity, in order to create ionic substitution defects in the TiO_2 lattice during growth and to improve the dielectric properties (permittivity and conductivity) of the synthesized TiO_2 (pure TiO_2 had weak electrorheological response).[38, 43] The pH of the colloidal solution after addition of the cake was measured to be between 1 and 2. Peptization occurred after heating the product at 80 °C for 1 h under medium stirring, whereupon the slurry became a stable sol. Then the sol was cooled down to room temperature and a 17 M ammonium hydroxide solution was added drop by drop into the TiO_2 sol under low stirring in order to form a white gel. The pH of the resultant colloidal suspension was measured to be close to 7. The gel was then collected by centrifugation (10000 g for 30 min) and dried at 110 °C overnight. The powder was crushed and ground into fine powder using a mortar and pestle and was further calcined in air at 500 °C for 4 h.

2-b Particles characterization

Morphological characterization of the obtained TiO_2 was shown in **Figure 1**. TEM pictures performed on the obtained TiO_2 particles in aqueous medium at pH≈ 7 (**Figure 1 (a) and (a')**) showed spherical particles with a diameter between 12 and 20 nm that were aggregated between them in a form of large clusters having a weak density. After heat treating TiO_2 powder at 500 °C for 4h in air, the SEM picture (**Figure 1 (b)**) showed relatively dense aggregates formed from the TiO_2 nanoparticles. The density of the calcined TiO_2 was measured using a 5 cm^3 standard flask pycnometer and was found to be about 3.84 g cm^{-3}. The type of porosity and specific surface area of the calcined TiO_2 powder were
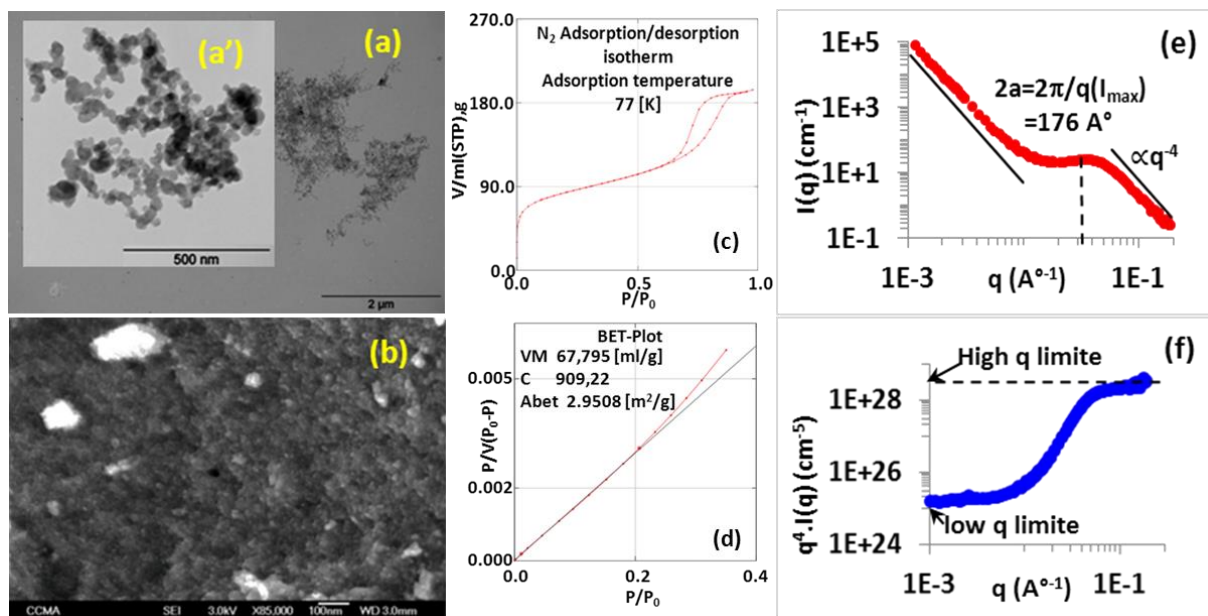
Figure 1: Morphological characterization of synthesized TiO$_2$ particles: **(a)** TEM picture of the dilute TiO$_2$ suspension as obtained at pH 7; inset **(a')** TEM picture of the same TiO$_2$ with a magnified scale, **(b)** SEM picture of TiO$_2$ after heat-treatment at 500 °C, **(c)** and **(d)** are the N$_2$ adsorption/desorption isotherm and the BET plot of N$_2$ adsorption performed on the calcined TiO$_2$ powder, respectively, **(e)** and **(f)** the SANS spectra of TiO$_2$ powder (calcined at 500°C/4h) dispersed in PDMS silicone oil (20 v. %) giving, respectively, the scattered intensity Iq (cm^{-1}) versus wave vector q (A$^{\circ-1}$) and the corresponding Porod representation q^{4}Iq (cm^{-5}) as a function of wave vector q (A$^{\circ-1}$).

determined by a N$_2$ adsorption/desorption technique. **Figure 1 (c)** shows a hysteresis in the N$_2$ adsorption/desorption isotherm for relative pressures $0.55 < P/P_0 < 0.95$ which is a typical characteristic of mesoporous or nanoporous aggregates. The BET plot of N$_2$ adsorption/desorption (**Figure 1 (d)**) showed that the value of the specific surface area of TiO$_2$ powder (Abet) was about 295 m^{2}g^{-1}. Small angle neutron scattering (SANS) was performed on calcined TiO$_2$ particles that were dispersed in PDMS oil (20 v. % TiO$_2$/PDMS). The SANS spectra giving the scattered intensity I$_q$ (cm^{-1}) versus wave vector q (A$^{\circ-1}$) (**Figure 1 (e)**) showed a relative maximum of the scattered intensity for a value of wave vector q about 0.356 nm^{-1} giving an average diameter of TiO$_2$ nanoparticles close to 18 nm which was in agreement with that estimated from TEM observations. The Porod plot of the scattered intensity q^{4}I$_q$ (cm^{-5}) as a function of the scattering wave vector q (A$^{\circ-1}$) (**Figure 1 (f)**) showed two Porod's regimes: the first at low wave vector which characterizes the interface of the

envelope of micrometric grains and the second at high q values which was due to the scattering inside the nanoparticles of 18 nm of diameter. This behaviour is characteristic of porous systems formed from nanoparticles assembling where two length scales were largely separated; nanoparticles on one hand and micrometric grains on the other.

2-c Preparation of the TiO_2 ERE
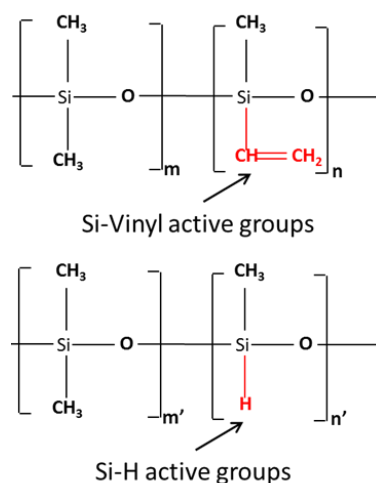
Figure 2: The chemical structure of PDMS crosslinking pre-polymers.

TiO_2 particles were introduced into a cross-linkable liquid composition comprising two polysiloxane (PDMS) constituents: as shown in **Figure 2**, one of them carrying Si-vinyl groups and the other carrying Si-H groups. Crosslinking by hydrosilylation reaction was initiated thermally and with a platinum-based catalyst. These cross-linking materials (cross-linking agents and catalyst) were integrated into two separated containers, Rhodorsil RTV141 A, viscosity 3.5 Pa.s, density 1.02 g cm^{-3} at 25 °C and Rhodorsil RTV141 B, viscosity 0.65 Pa.s, density 1.02 g/cm^3 at 25 °C, that were purchased from Bluestar Silicones. To 10 parts of Rhodorsil RTV141 A were added 1 part of Rhodorsil RTV141 B in order to obtain the crosslinking reactions with a molar stoichiometry of groups, Si-vinyl / Si-H close to 1. The amount of TiO_2 particles was fixed at 50 wt. % (~20 v. %) in the whole mixture then a few drops of acetylacetone was added to the mixture (the Acac amount was less than 1.5 wt. % in order to obtain surface adsorption of Acac/TiO_2 ≤ 1Acac molecule per nm^2). The process consisted of introduction and vigorous mixing of TiO_2 powder, Acac and Rhodorsil RTV141

A in a mortar until obtaining a homogeneous dispersion, then the mixture was degassed under vacuum for 30 min using a vacuum pump for removing any air bubbles that may be traped in the mixture. At this stage no crosslinking reaction was started. The Rhodorsil RTV141 B component was then added to the mixture. After homogenizing the whole by mechanical stirring, the dispersion was degassed again for 5 min and then rapidly poured onto the rheometer plateau to monitor the crosslinking reaction (controlled by temperature and time) with or without an applied electric field under shear.

2-d Electrorheological measurements

The viscoelastic properties were measured by using an Anton Paar Physica MCR301 rheometer which was equipped with an electrorheological temperature device (Anton Paar) consisting of a parallel plate geometry of 25 mm diameter (PP25/E) and a Peltier temperature device (P-PTD200/E) allowing rheological measurements under applied electric field with thermally controlled environment. A regulated DC power supply (XANTREX-Model HPD 30-10SX) and AC voltage (Hameg function generator HM8030-5) combined with a high voltage amplifier (Trek Model 609E-5) were used to apply DC or AC electric field in the range of 0 to 4 kV/mm across a 1 mm gap between plate geometries. Multimeter (TENMA 72-7735) was used to measure the DC or AC electric current passing through the gap during crosslinking under applied electric field and rheological monitoring.

3. Results and discussion

3-a Cross-linking kinetics with and without an applied electric field:

The polymerization kinetics of the TiO_2-Acac particles-filled PDMS (20 v. % TiO_2-Acac filler in reacting PDMS) was monitored by measuring the storage and loss moduli during cross-linking reaction at constant strain magnitude $\gamma=0.1$ % and $\omega=100$ rad/s. the crosslinking reaction is carried out at a constant temperature of 80 °C. The experiments were carried out under three different conditions. In one, pure PDMS pre-polymers were cross-linked without
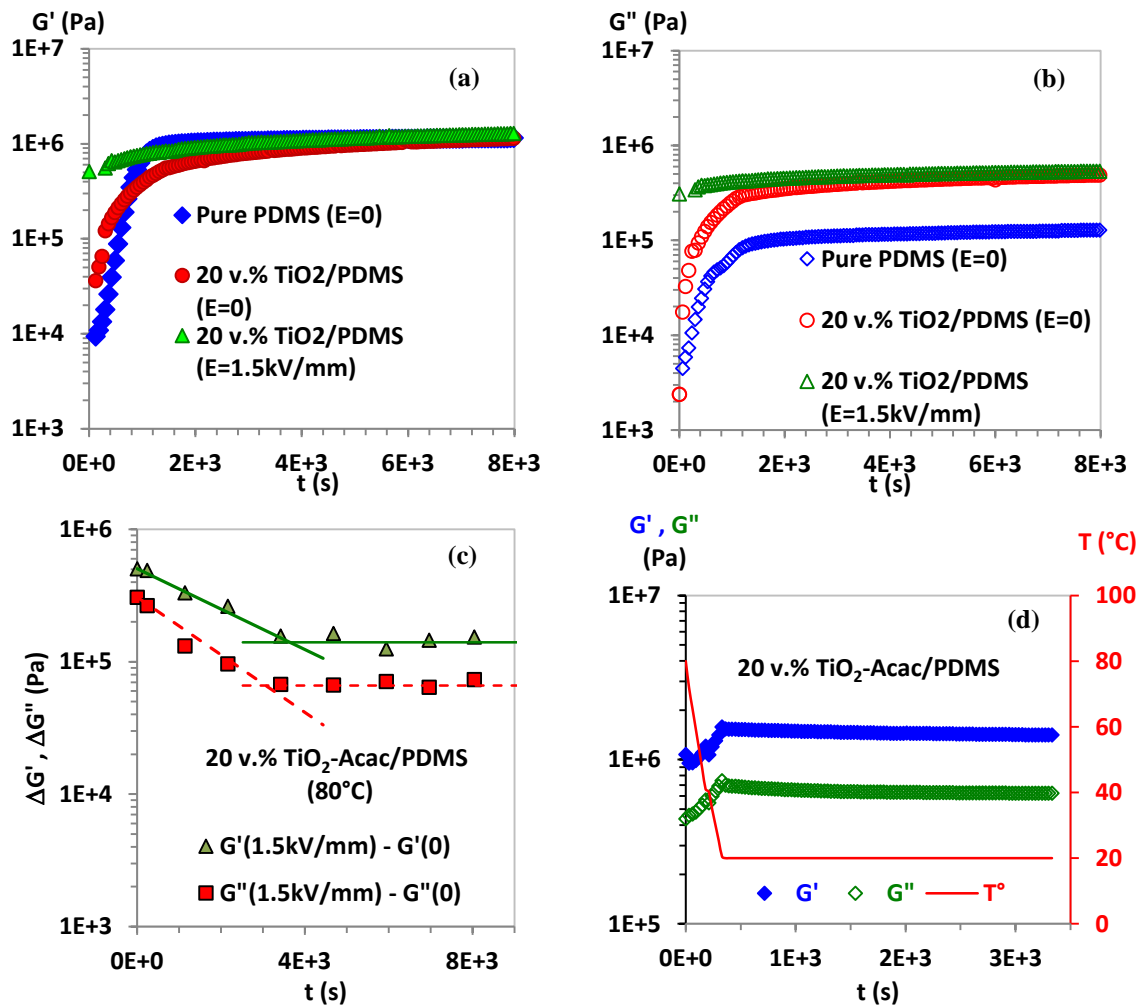
Figure 3: TiO$_2$ ERE cross-linking kinetics, **(a)** G' of pure PDMS and G' of 20 v. % TiO$_2$/PDMS without pre-alignement (E=0kV/mm) and with pre-alignement at E=1.5 kV/mm AC electric field strength (v$_{ac}$=10 Hz), **(b)** G" of pure PDMS and G" of 20 v. % TiO$_2$/PDMS with and without pre-alignement, **(c)** $\Delta G'=G'_{E=1.5kV/mm}- G'_{E=0}$ and $\Delta G''= G''_{E=1.5kV/mm}- G''_{E=0}$ during cross-linking of 20 v.% TiO$_2$/PDMS, **(d)** variation of G' and G" of the TiO$_2$-Acac/PDMS ERE after the end of cross-linking (at E= 0 kV/mm) versus time as the sample was cooled down (linear ramp of temperature from 80 to 20°C) and maintained at constante T= 20°C. Shear moduli are measured at strain amplitude γ= 0.1 % and ω=100 rad/s and for fig. (a), (b) and (c) the temperature was fixed at T=80°C.

particles and in the second one, TiO$_2$-Acac particles were randomly distributed in PDMS pre-polymers without pre-alignment during crosslinking. In the third one an AC electric field strength of 1.5 kV/mm with a frequency of 10 Hz was applied to pre-align the particles in PDMS precursors before starting polymerization and was maintained during the entire cross-linking reaction time. The use of an AC electric field was deliberately chosen to prevent the electrophoretic transport towards electrodes (phase separation resulting from the accumulation

of the particles on the electrode surfaces) that may occurred by applying a DC electric field in the first step of crosslinking process (where the dispersion is still fluid). **Figures 3 (a)** and **3 (b)** show that both G' and G" of pure PDMS increase from a few kPa to their equilibrium values (G'=0.90 MPa and G"= 87 kPa) for t= 1260 s. However in the presence of 20 v. % TiO_2-Acac filler in reacting PDMS pre-polymer (without pre-alignment), the cross-linking rate was slowed significantly with G' and G" (of 20 v. % TiO_2-Acac/PDMS) reaching equilibrium after 3300s. We assumed that the addition of TiO_2-Acac filler caused the reduction of the activity of platinum catalyst complex and then the reduction of the cross-linking rate. After reaching the equilibrium, we observed no significant difference in the storage moduli G' of both pure PDMS and 20 v. % TiO_2-Acac/PDMS, while additional energy dissipation was observed in TiO_2-Acac/PDMS network (**Figure 3 (b))** where its loss modulus G" was about 4.8 time higher than that of pure PDMS. **Figure 3 (a)** and **3 (b)** show a comparison of the cross-linking kinetics between TiO_2-Acac/PDMS without an applied electric field and pre-aligned TiO_2-Acac/PDMS with an applied electric field. With an applied AC electric field (E=1.5 kV/mm and ν=10 Hz) the nominal ER response of the TiO_2-Acac/PDMS in its fluid phase (before starting cross-linking at t=0 s) was about G'=0.50 MPa and G"=0.30 MPa; then both G' and G" were increased during the crosslinking time until reaching their equilibrium values (G' = 1.04 MPa and G" = 0.486 MPa) at t=3300 s. However, before reaching the equilibrium, the increase on G' and G" under the applied electric field was less pronounced than that without pre-alignment or in other words we did not have the addition of the part of modulus induced by the electric field (at t = 0) and the one given by the polymerization of the PDMS network. This behaviour can be easily seen in **Figure 3 (c)** where the relative change during time, $\Delta G'=G'_{E=1.5kV/mm}- G'_{E=0}$ and $\Delta G"= G"_{E=1.5kV/mm}- G"_{E=0}$, was decreased exponentially until reaching the equilibrium values $\Delta G'=0.140$ MPa and $\Delta G"=0.0660$ MPa. This decrease of $\Delta G'$ and $\Delta G"$ may be attributed to the moderate value of the applied AC electric field ($E_{ac}=1.5$ kV/mm at10 Hz), which does not
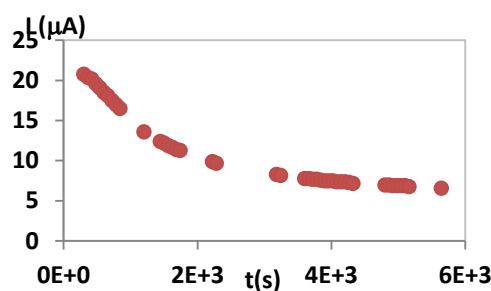
Figure 4: Evolution of the current during cross-linking at constant T=80 °C under rheological monitoring of the TiO_2-Acac/PDMS ER with pre-alignment under an applied AC amplitude E=1.5 kV/mm and ν_{ac}=10 Hz.

prevent the particles from moving during the polymerization stage, thus reducing the electrostatic forces. As shown in **Figure 4**, the limited amplitude of the applied AC electric field was due to the high conduction of the sample at 80 °C in the first stages of crosslinking where the sample remained still fluid or partially cross-linked preventing the application of high electric field strength. The equilibrium values of ΔG' and ΔG" were reached at the same time (t~3300 s) as the electric current of the sample tends to a lower limit of 7 µA. After the end of polymerisation, the sample was cooled down from 80 °C to 20 °C, and we measured G'(0) and G"(0) at the constant temperature of 20 °C during several minutes to ensure that both G'(0) and G"(0) reached their stable values (**Figure 3 (d)**). We noticed that by cooling down the sample to 20 °C, G'(0) and G"(0) were increased from respectively 0.90 MPa and 0.066 MPa to reach 1.50 MPa and 0.70 MPa. After reaching the stable values of G'(0) and G"(0) at 20 °C, the resulting elastomers were characterized by FT-IR spectroscopy to monitore the cross-linking reaction. the FT-IR spectra of both TiO_2-Acac/PDMS and pure PDMS elastomers showed that the characteristic absorption peaks of the Si-H groups (that are present in the FT-IR spectra of cross-linking pre-polymer) disappear completely confirming the total consummation of the Si-H groups by hydrosilylation and hence, the relatively high density of the obtained elastomer network with G'(0) =1.5 MPa (more details about FT-IR characterization of samples are available in electronic supplementary information).

**Table 1:** dielectric properties measured at 20 °C

	PDMS matrix	TiO₂ Particles
ε_r	2.7 *	120
σ (S.m^{-1})	1 10^{-13} *	2.50 10^{-7}

* Data from provider.

In subsequent experiments, the viscoelastic properties were measured at a fixed temperature of 20 °C, for different values of DC electric field strength, electric field frequency and oscillatory shear strain magnitude. The dielectric properties (conductivity and relative permittivity) of both TiO₂ particles and crosslinked matrix were given at the same temperature of 20 °C and are shown in **Table 1**.

3-b The DC Electric field-dependency of electrorheological response of the TiO₂-Acac /PDMS ERE:

Shear moduli (G' and G") were measured under shear strain magnitude, γ=0.1 % and ω=100 rad/s, as a function of the applied DC electric field strength. The experiments consisted of applying suddenly a DC electric field and maintaining it during 270 s before turning off the field; the change of the moduli was recorded during this field pulse. The effect of the field on moduli under various DC electric field strengths was reported in **Figure 5**. We observed in parts **(a)** and **(b)** an instantaneous increase of G' and G" when the DC electric field was applied. As shown in **Figure 5 (c)**, where the dash-dotted curve corresponds to a linear behaviour, the relative change in elastic modulus [ΔG'=G'(E)-G'(0)] was nearly proportional to the applied DC electric field E_{dc} and not to the quadratic law $(E_{dc})^2$ as it should be the case for linear electrostatics. J. N. Foulc et al. (1994) attributed this deviation from linear electrostatics to the fact that, under DC voltage, the conductivity of the matrix became field-dependent and was dramatically increased when a certain local field strength E_m was exceeded; then the attraction force F_{elec} between particles and the storage modulus enhancement G'_{elec} at a small strain magnitude became proportional to E_{dc}.[11,13,14] In our case, from the experimental results, we found that $\Delta G' \propto E_a^{1.10}$ (**Figure 5 (c)**). A similar exponent
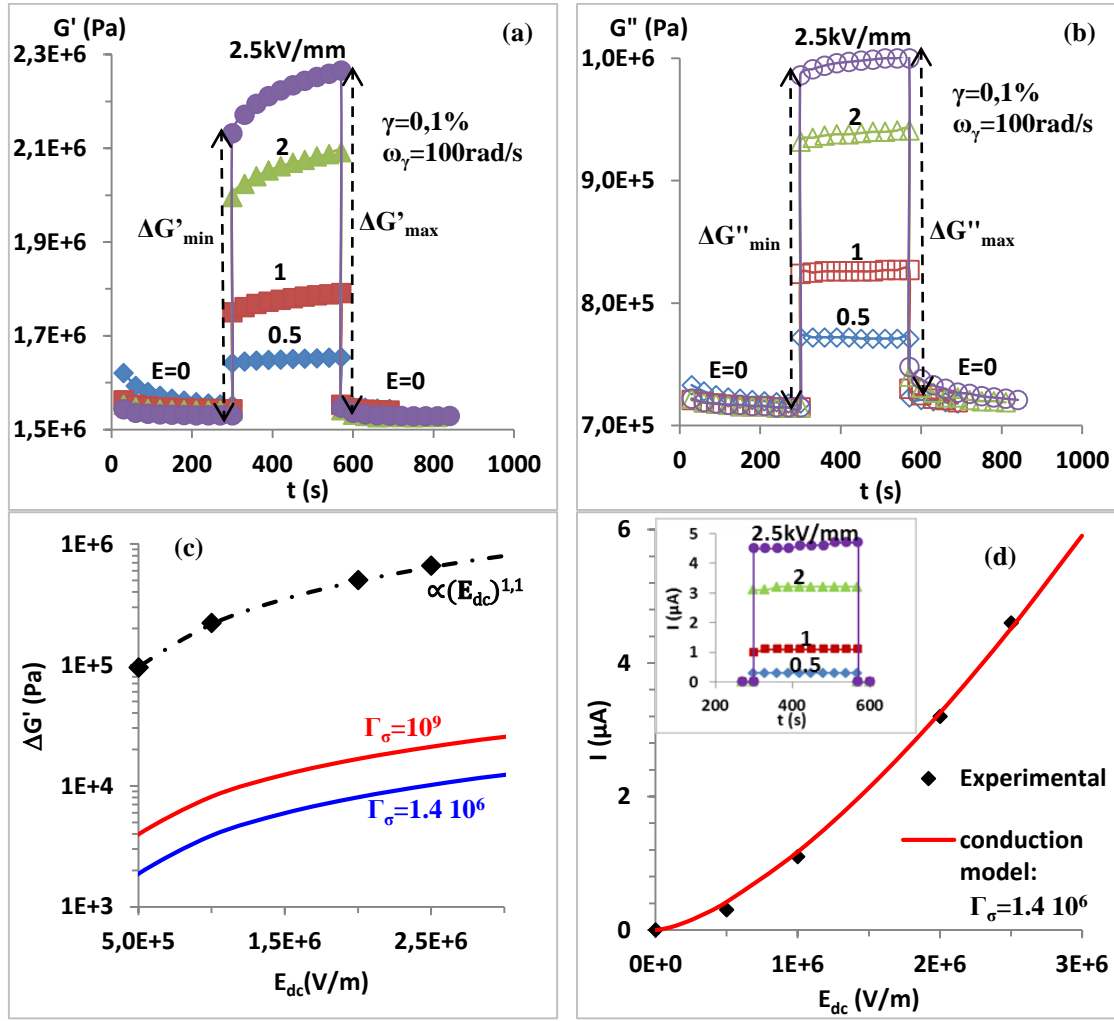
Figure 5: the DC electric field dependence of the storage modulus and loss modulus by applying the switching electric fields of different values; **(a)** variation of G' **(b)** variation of G" **(c)** the relative change in elastic modulus: diamond: experimental values, blue and red lines: calculated ΔG' using eq. (4) for conductivity ratios $\Gamma_\sigma = 1.4\ 10^6$ and $\Gamma_\sigma = 10^9$ respectively, dash-dotted curve corresponds to $\Delta G' \propto E_{dc}^{1.1}$, **(d)** variation of the current as a function of the applied electric field; diamond: experimental values, red line: calculated current using equation (3) for $\Gamma_\sigma = 1.4\ 10^6$ (inset the variation of the current as a function of application time of a constant electric field for the different applied E_{dc}).

of attraction force dependence on the electric field was predicted by Gonon et al. (1999) at a high applied field where the saturation regime was reached and they found that $F_{elec} \propto E_{dc}^{1.12}$.[11] However **Figure 5 (a)** shows a difference in the measured *ΔG'* between its value just after the application of the field at t=t$_0$ (that we call ΔG'$_{min}$) and after t=270 s of electric field induction (that we call ΔG'$_{max}$); in particular when the DC applied electric field strength became strong. This evolution during the time of application of the field could not be attributed to the current variation because, as shown in the inset **(d)** of **Figure 5**, the current was practically

unchanged during this time even at high applied electric field strength. The more likely explanation is the existence of a slow rearrangement of the particles which get closer from each other, then increasing the moduli. Theoretical estimation of the variation of the current and the attraction force as a function of the applied electric field has been given in the literature using the conduction model. [14, 15] In this model the authors considered, for the case where the ratio of the conductivities $\Gamma_\sigma = \sigma_P/\sigma_M \gg 1$, that the electrical conduction in the interparticle gap can be separated into two zones for nearly touching particles (see **Figure 6**). The first one, dominated by the conductivity σ_P of the particles; had a radius δ. The second one was the outer zone ($x > \delta$) where authors considered that the sphere surfaces are equipotential and that, at a high applied electric field, the conductivity of the matrix became field-dependent. The radius δ was determined by equating $C_P = C_M$ where C_p and C_M are respectively the conductance associated with these two zones: $x < \delta$ and $x > \delta$.
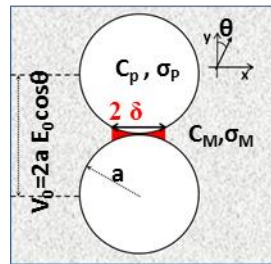
Figure 6: Schematic view showing the electrical conduction zones and notations used in the conduction model.
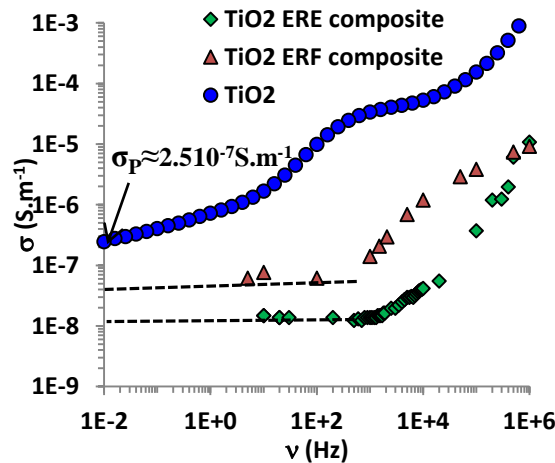
Figure 7: Experimental measurement of the conductivity; circle: $\sigma_P = \sigma_{pellet}/\Phi_v$ ($\Phi_v = 0.44$),

triangle: suspension TiO$_2$-Acac/ PDMS ERF Φ_v=0.20 and diamond: TiO$_2$-Acac/PDMS ERE Φ_v=0.21.

In this model the radius δ was practically proportional to $E_{dc}^{0.5}$ but decreased with the conductivity ratio as $\delta \propto (ln\Gamma_\sigma)^{-1}$.

The attraction force between two nearest particles was expressed as:

$$F_{elec} = 4\pi a^2 \varepsilon_M E_{dc}^2 \left(a/\delta\right)^2 \quad (1)$$

In equation (1), the attraction force increases by decreasing δ and therefore by increasing Γ_σ.

Using the conduction model, the dependence between the applied electric field E_{dc} and the current I_P passing through a single chain of aligned particles was derived in the case of near touching particles and was expressed as: [15,16]

$$I_P = 4\pi a\sigma_P(2aE_{dc})^2 \sqrt{\varepsilon_M/F_{elec}} \quad (2)$$

The total current I passing through all the chains was expressed as:

$$I = N_{Chains}I_P = \frac{3}{2}\phi\left(\frac{R}{2a}\right)^2 I_P \quad (3)$$

where ϕ is the particle volume fraction and R is the radius of the plate geometry used on the rheometer (R=12.5 10^{-3} m).

Inserting (1) and (2) into equation (3) we found that $I \propto \frac{E_{dc}^2}{\sqrt{F_{elec}}} \propto E_{dc}^{1.5}$.[15,16] **Figure 5 (d)** shows a comparison between the experimental and calculated results using equation (3) for the current passing through the sample. The best fit was obtained for a conductivity ratio Γ_σ= 1.4 10^6 giving σ_P=1.4 10^{-7} S.m^{-1}. The conductivity of TiO$_2$/Acac was deduced from the measurement of the conductivity σ_{eff} of a pellet of TiO$_2$ having a volume fraction Φ_v=0.44. We assumed that σ_P= σ_{eff}/ Φ_v. The frequency dependence of σ_P as well as the conductivity of the suspension before and after polymerization is represented in **Figure 7**. We noticed in particular that, as expected, the conductivity was strongly decreased in the elastomer but that

the frequency dependency is quite similar in the liquid phase and in the elastomer. The experimental conductivity ratio at a low frequency was then equal to $\Gamma_\sigma = 2.5 \cdot 10^6$ which is not so far from the one $1.4 \cdot 10^6$ deduced from the fit of the model, taking into account the uncertainty due to the approximation $\sigma_P = \sigma_{eff}/\Phi_v$. The relative change in the storage modulus can be obtained as follow:[13]

$$\Delta G' = \frac{3}{2}\phi\frac{1}{\pi a^2}\frac{F_{elec}}{(1+\gamma^2)} \quad (4)$$

The shear strain γ appearing in equation (4) can be neglected in our case. Experimental results of $\Delta G'$ versus the DC applied electric field are compared with those calculated by inserting equation (1) into (4). **Figure 5 (c)** shows that both experimental and computed results had practically the same dependence on the electric field where $\Delta G' \propto E_{dc}^{1.1}$. However theoretical estimation of $\Delta G'$ is lower by about two orders of magnitude compared to our experimental results even if the conductivity ratio Γ_σ was increased to 10^9 (**Figure 5(c)**). This high value of $\Delta G'$ observed on nanoparticles coated with molecules of high dipole moment could come from the variation of the force at very short separation. In the approach leading to Equation (4) the change of force with the separation distance dF/ds is not considered since only the projection of the constant force near contact on the shear direction is taken into account. The short range force should also include the Van der Waals interaction and likely interactions between dipoles adsorbed on the surface of the particles. This is beyond the scope of this paper but certainly worth being explored.

As shown in **Figure 5 (a)** or **5 (c)**, the relative change in storage modulus ($\Delta G' = G'(E) - G'(0)$) of TiO$_2$-Acac/PDMS ERE exhibited high values when compared with those of other ER Elastomers that have been investigated before (**Table 2**). For example, for a DC applied electric field of 2 kV/mm, oscillatory shear strain $\gamma = 0.1$ % and $\omega = 100$ rad/s, TiO$_2$-Acac/PDMS ERE response reached the $\Delta G'$ value up to 0.5 MPa. This high performance of TiO$_2$-Acac/PDMS ERE was attributed to the particular morphology of the synthesized TiO$_2$

Table 2: Relevant recently published studies on the viscoelastic properties of the ERE under a DC applied electric field.

ERE sample	E_{dc}	$\gamma(\%)$; ω(rad/s)	G'(0)(KPa)	ΔG' (kPa)	Γ_σ	Γ_ϵ	T°(K)	Ref.
TiO$_2$-Acac/PDMS 50 wt.%	2 kV/mm	0.1; 100	~1500	~500	~2.50 10^6	~44	293	This work
PANI/PDMS 30 wt.%	2 kV/mm	0.1; 100	~30	~110	-	-	-	22
PbTiO$_3$/AR71 21.30 wt. %	2 kV/mm	0.1; 100	~45	75-85	~4.39 10^{5*}	~3.80 10^{3*}	300	26
Starch/Transformer oil/ silicone rubber (5/47.5/47.5 wt. %)	0.6 kV/mm	0.05; 6.280	~20	81.7	-	-	293	27
Starch/silicone oil/silicone rubber (10/45/45 wt. %)	0.6 kV/mm	0.05; 6.280	~37.21	90.8	-	-	293	28
Polythiophene/polyisoprene 20 wt. %	2 kV/mm	1; 1	~19.45	~21.40	~3.67	-	300	29
Pb(Zr$_{0.5}$,Ti$_{0.5}$)O$_3$/acrylic rubber	2 kV/mm	0.1; 1	~ 18.80	~11.02	~1.92 10^{5*}	~1.6510^{3*}	300	30
Polydiphenylamine/poly(styrene-block-isoprene-block-styrene) 20 v. %	2 kV/mm	0.1; 1	~ 88.77	~123.32	~2.26 10^{13}	-	300	31
Poly(p-phenylene)/ acrylic elastomer 30 v. %	2 kV/mm	0.1; 1	110.99	~107.80	~2.25 10^6	-	300	32
Cellulose/BMIMCl 13 wt. % gel	1 kV/mm	0.1; 1	172.22	248	-	-	303	33

* The conductivity and relative permittivity ratios are measured at 1 kHz.

- Data are not provided by the authors.

particles (mesoporous aggregates with a high specific area of 295 m^2/g formed from nanosized particles) and to the good affinity between TiO$_2$ surface and acetylacetone allowing the adsorption of 1 molecule per nm^2 of Acac dipolar molecules on the TiO$_2$ surface with practically no Acac remaining free in the insulating matrix.[42] If we considered the relative change of modulus, defined as *ΔG'/G'(0)(%)=100(G'(E)-G'(0))/G'(0)*, its value remained modest (33% as shown in **Table 2** for 2 kV/mm, γ=0.1%) but it was just due to the high intrinsic modulus of the PDMS matrix obtained using the RTV141 reacting pre-polymers with a molar stoichiometry of groups, Si-H /Si-vinyl close to 1. The intrinsic elasticity of the PDMS matrix can be easily decreased by adding an adequate molecular agent (trimethyl (vinyl) silane for instance) to neutralize some of the Si-H groups and to reduce Si-H/Si-Vinyl molar stoichiometry. In this case the elastic modulus of the matrix will decrease whereas the effect of the field will remain constant, so the storage modulus sensitivity (*ΔG'/G'(0)*) can be strongly modulated depending on the needs of the applications. In our experiment, the relative change ΔG' of TiO$_2$-Acac/PDMS at its fluid phase (before starting cross-linking) was about 0.70 MPa by the application of electric field strength of 2 kV/mm and after the end of the

cross-linking reaction this value was decreased to 0.5 MPa at the same applied electric field. If the matrix is softer, then we expect that ΔG' of TiO$_2$-Acac/PDMS in its elastomeric phase will increase to be closer to that of TiO$_2$-Acac/PDMS in its fluidic phase.

3-c Electric field frequency dependency of the electrorheological response of TiO$_2$-Acac/PDMS ERE:

Experiments were carried out to measure G' and G" of TiO$_2$-Acac/PDMS ERE, under shear strain magnitude γ=0.1 % and ω=100 rad/s, depending on the electric field frequency. In **Figure 8** we show the increase of modulus obtained by applying an electric field strength E=2 kV/mm for 270 s with different frequencies on the crosslinked TiO$_2$-Acac/PDMS ERE. **Figures 8 (a)** and **(b)** show again a large increase of the storage and loss moduli when the AC field was turned on at a value of 2 kV/mm and different frequencies nevertheless it was less important than the value obtained in the DC field and it continuously decreased with frequency. The dependence of mechanical properties on electric field frequency can be determined by giving the variation of the attractive force as a function of frequency. In the case of nearly touching particles and $\Gamma_\sigma=\sigma_P/\sigma_M > \Gamma_\varepsilon=\varepsilon_P/\varepsilon_M$, the attraction force can be expressed as:[10,13]

$$F_{elec} = 12\pi a^2 \varepsilon_M |\beta^*|^2 \exp(2|Re(\beta^*)|^{32}) E_0^2 \qquad (5)$$

where $|\beta^*|^2$ and $|Re(\beta^*)|$ depend on the dielectric properties of the particles and the matrix and vary with frequency as:

$$|\beta^*|^2 = \frac{\frac{(\sigma_p-\sigma_M)^2}{\omega^2\varepsilon_0^2}+\left(\varepsilon_r^P-\varepsilon_r^M\right)^2}{\frac{(\sigma_p+2\sigma_M)^2}{\omega^2\varepsilon_0^2}+\left(\varepsilon_r^P+2\varepsilon_r^M\right)^2} \qquad (6)$$

$$\text{and } |Re(\beta^*)| = \frac{\omega^2\varepsilon_0^2\left(\varepsilon_r^P-\varepsilon_r^M\right)\left(\varepsilon_r^P+2\varepsilon_r^M\right)+(\sigma_p-\sigma_M)(\sigma_p+2\sigma_M)}{\omega^2\varepsilon_0^2\left(\varepsilon_r^P+2\varepsilon_r^M\right)^2+(\sigma_p+2\sigma_M)^2} \qquad (7)$$

Therefore, the relative change in storage modulus can be calculated by inserting the expression of F$_{elec}$ given in equation (5) into equation (4). Using these expressions, the authors
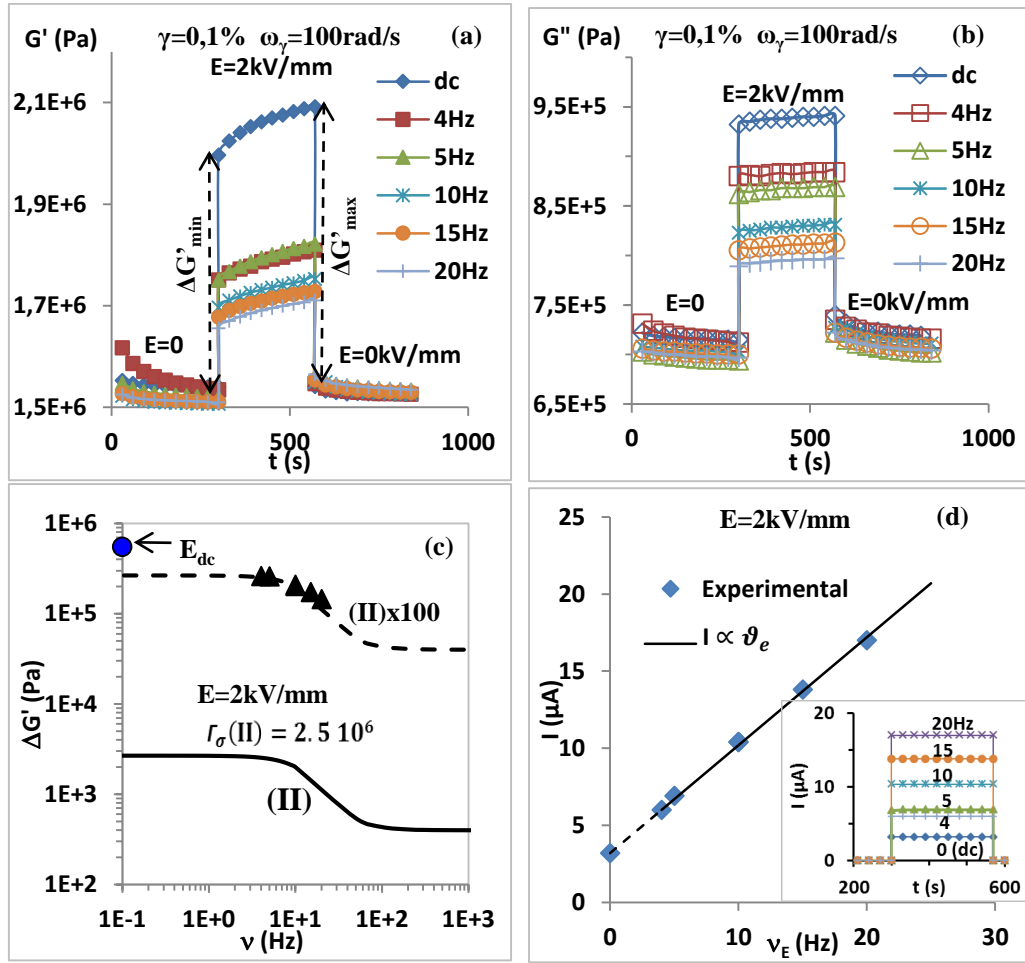
Figure 8: the applied electric field frequency dependence of the storage modulus and loss modulus after switching on the electric field; **(a)** the time dependance of G' for different electric field frequencies, **(b)** the time dependance of G'' for different electric field frequencies, **(c)** the relative change in the elastic modulus versus the applied electric field frequency (triangles: experimental results; solid line: theory with $\Gamma_\sigma = 2.5 \ 10^6$; dashed line: theoretical results multiplied by 10^2, **(d)** the corresponding electric field current versus electric field frequency; inset: the variation of the current during field application for the different electric field frequencies.

found that the attractive force and then the elastic modulus had a higher value at DC and very low frequencies, but became frequency dependent and decreased when electric field frequency was increased beyond a critical value. They demonstrated that the parameters determining this critical frequency limit were the conductivity ratio Γ_σ and the dielectric permittivity ratio Γ_ε. They also found that the calculated current was independent of the electric field frequency when the frequency was smaller than a critical value, but became a linear function of the frequency beyond the critical value. For $\Gamma_\sigma = 10^6 \gg \Gamma_\varepsilon = 5$ the authors found that the critical value of the frequency was very low and was less than $6.7 \ 10^{-4}$ Hz. In

our case $\Gamma_\sigma \sim 2.5 \ 10^6 >> \Gamma_\varepsilon \sim 44$, we observed the decay of G' and ΔG' (**Figure 8 (a)** and **(c)**) by increasing the frequency and a linear behaviour of the current I versus frequency (**Figure 8 (d)**). We noticed that the decrease of ΔG' versus frequency around 10 Hz was well reproduced by the model as shown in **Figure 8 (c)**, but, as in the DC case, it underestimated (in the tested electric field frequency range) our experimental results by two orders of magnitude. Because of the limit of our instrument sensitivity at very low frequencies and because of the high conduction of the sample at high frequencies we were unable to produce much more experimental measurement points to investigate the transition regimes that were observed theoretically and therefore testing the validity of the model for simulating our experimental measurements over a wide range of frequencies.

In summary we found that the electrorheological behaviour of TiO$_2$-Acac/PDMS ERE was governed by the conductivity mismatch; with, for the TiO$_2$-Acac/PDMS ERE, a higher ER response by applying a DC electric field than an AC one.

3-d Strain dependency of the electrorheological response of the TiO$_2$-Acac/PDMS ERE:

The linear viscoelastic regime of the TiO$_2$-Acac/PDMS ERE was investigated by measuring ΔG' and ΔG'' as a function of oscillatory shear strain magnitude (γ) at constante shear frequency $\omega_\gamma = 100 \ rad/s$. We carried out measurements without an electric field, with a *2.5 kV/mm* DC and 2 kV/mm AC electric field *($\nu_E = 10 \ Hz$)*. In **Figure 9** we can see that with or without an applied electric field, the TiO$_2$-Acac /PDMS ERE had a small linear regim for $\gamma \leq 0.1 \ \%$, which was independent of DC or AC modes but was dependent on the electric field strength. This small linear regime could be attributed to the infinitesimal deformation of columns of aligned particles locked in the cross-linked matrix that influenced the viscoelastic properties.[22] We noticed also (in **Figure 9**) that, increasing the electric field strength from 2 to 2.5 kV/mm, the linear regime was disappeared. This evolution of nonlinearity by increasing the electric field strength is likely related to the increase of conductivity: the size of the zone $r < \delta$ (cf **fig.(6)**) extends with the electric field and makes the modulus sensitive to very small

strain.
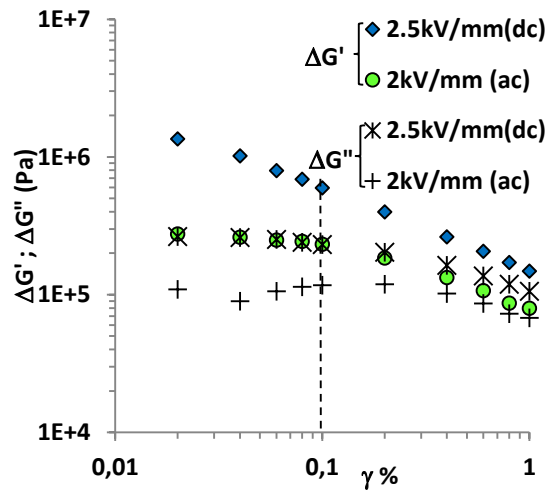
Figure 9: Strain dependence of ΔG': (closed diamond) E_{dc}=2.5 kV/mm, (closed circle) E_{ac}=2 kV/mm (ν_E=10 Hz), and ΔG": (stars) E_{dc}=2.5 kV/mm, (plus symbols) E_{ac}=2 kV/mm (ν_E=10 Hz).

4. Conclusion

ER elastomers have been prepared by suspending TiO$_2$-doped Acac particles in cross-linkable PDMS oligomers. The particles were aligned by an AC electric field and maintained in chain like structure by an in situ polymerization to form anisotropic network. The change of the shear modulus was monitored during the polymerization process and its decrease was less than 30% indicating that the field induced structure was only slightly disturbed by the polymerization process. Electrorheological properties of TiO$_2$-Acac/PDMS ERE were investigated experimentally under a DC electric field, AC frequency and shear strain magnitude. The results showed that the relative change in elastic modulus (ΔG') increases with the DC applied electric field according to a power law $\approx E^{1.10}$. this deviation from the quadratic law is due to the non linearity in the conductivity of the matrix that affects the field distribution and the attraction force between particles. However TiO$_2$-Acac/PDMS ERE showed a decrease of ΔG' with the increasing AC electric field frequency. This viscoelastic behaviour, depending on the electric field frequency, was attributed to the high conductivity ratio $\Gamma_\sigma=\sigma_P/\sigma_M$ compared to the permittivity ratio $\Gamma\varepsilon=\varepsilon_P/\varepsilon_M$, between TiO$_2$ semiconducting particles and PDMS matrix. TiO$_2$-Acac/PDMS ERE exhibited a high value of relative change

in the elastic modulus ΔG' when compared with those of other ER Elastomers that have been investigated before; ΔG' reached 500 kPa under 2 kV/mm of a DC applied electric field at a strain *γ=0.1 %.* Whereas the conductivity behavior can be quite well predicted by the field dependence on the conductivity this was not at all the case for the increase of the shear modulus where the theory predicted a value which was too small by 2 orders of magnitude; a better consideration of short range forces is needed to improve the model. The high ER performance of TiO_2-doped Acac as an ERE makes it a promising candidate for applications by designing an elastomeric blend with controllable matrix hardness.

Supporting information. Electronic supplementary information (ESI) available: The experimental setup for morphological characterization (SEM, TEM, N_2 adsorption/desorption isotherm, SANS and FT-IR) and dielectric characterization by impedance spectroscopy. See DOI: 10.1039/c4tc02535k on www.rsc.org/MaterialsC website.

References

[1] M. Behrooz, X. Wang and F. Gordaninejad, Performance of a new magnetorheological elastomer isolation system, *Smart Mater. Struct*., 2014, 23, 045014

[2] I. Bica , Y. Dan Liu and H. J. Choi, Magnetic field intensity effect on plane electric capacitor characteristics and viscoelasticity of magnetorheological elastomer, *Colloid Polym. Sci*., 2012, 290,1115–1122

[3] K.Tanaka, R. Akyama, Electrically Induced Microstructures in Micro and Nano-Suspensions and Related Physical Properties, *Journal of Physics: Conference Series*, 2009, 149**,** 012097

[4] R. A. Anderson, Electrostatic forces in an ideal spherical-particle electrorheological fluid, *Langmuir*, 1994, 10, 2917-2928

[5] M. Parthasarathy and D. J. Klingenberg, Electrorheology: mechanisms and models, *Materials Science and Engineering*, 1996, R. 17, 57-103

[6] Howard See, Ryo Sakurai, Tasuku Saito, Shigeo Asai, Masao Sumita, Relationship between electric current and matrix modulus in electrorheological elastomers, *Journal of Electrostatics*, 2001, 50, 303-312

[7] Bo Liu and Montgomery T. Shaw, Electrorheology of filled silicone, *J. Rheol.*, 2001, 45(3), 641-657

[8] L. C. Davis, Polarization forces and conductivity effects in electrorheological fluids, *J. Appl. Phys.*, 1992, 72 (4), 1334-1340

[9] X. Tang, C. Wu, and H. Conrad, On the conductivity model for the electrorheological response of dielectric particles with a conducting film, *J. Appl. Phys.*, 1995, 78 (6),4183-4188

[10] C. W. Wu, and H. Conrad, Dielectric and conduction effects in ohmic electrorheological fluids, *J. Phys. D: Appl. Phys.*, 1997, 30, 2634-2642

[11] P. Gonon, J.-N. Foulc, P. Atten, and C. Boissy, Particle-particle interactions in electrorheological fluids based on surface conducting particles, *J. Appl. Phys.*, 1999, 86 (12), 7160-7169

[12] Howard See, Advances in modelling the mechanisms and rheology of electrorheological fluids, *Korea-Australia Rheology Journal*, 1999, 11 (3), 169-195

[13] C. W. Wu, and H. Conrad, A modified conduction model for the electrorheological effect, *J. Phys. D: Appl. Phys.*, 1996, 29, 3147-3153

[14] J.-N. Foulc, P. Atten, and N. Félici, Macroscopic model of interaction between particles in an electrorheological fluid, *J. of Electrostatics*, 1994, 33, 103-112

[15] P. Atten, C. Boissy and J.-N. Foulc, The role of conduction in electrorheological fluids: from interaction between particles to structuration of suspensions, *J. of Electrostatics*, 1997, 40 and 41, 3-12

[16] X. Tang, C. Wu, and H. Conrad, On the conductivity model for the electrorheological

effect, *J. rheol. Phys.*, 1995, 39 (5), 1059-1073

[17] Tohru Shiga, Akane Okada, and Toshio Kurauchi, Electroviscoelastic effect of polymer blends consisting of silicone elastomer and semiconducting polymer particles, *Macromolecules*, 1993, 26, 6958-6963

[18] Tohru Shiga, Takashi Ohta, Yoshiharu Hirose, Akane Okada, and Toshio Kurauchi, Electroviscoelastic effect of polymeric composites consisting of polyelectrolyte particles and polymer gel, *J. Mater. Sci.*, 1993, 28, 1293-1299

[19] Shisha Zhu, Xuepeng Qian, Hao He, Quanfu Zhang, Experimental research about the application of ER Elastomer in the shock absorber, *Advanced Materials Research*, 2013, vol. 641-642, 371-376

[20] Changyong Cao, and Xuianhe Zhao, Tunable stiffness of electrorheological elastomers by designing mesostructures, *Appl. Phys. Lett.*, 2013, 103, 041901

[21] Weihua Li and Xianzhou Zhang, Research and applications of MR Elastomers, *Recent Patents on Mechanical Engineering*, 2008, 1, 161-166

[22] Byung D. Chin, Myung-Suk Chun, H.Henning Winter, Modulus-switching viscoelasticity of electrorheological networks, *Rheol Acta*, 2009, 48, 177-189

[23] Yasuhiro Kakinuma, Tojiro Aoyama, Hidenobu Anzai, Application of the electro-rheological gel to fixture devices for micro milling process, *Journal of Advanced Mechanical Design, Systems, and Manufacturing*, 2007, Vol. 1, No. 3, 387-398

[24] James E. Martin and Robert A. Anderson, Electrostriction in field-structured composites: Basis for a fast artificial muscle?, *J. Chem. Phys.*, 1999, 111 (9), 4273-4280

[25] Kexiang Wei, Quan Bai, Guang Meng, and Lin Ye, Vibration characteristics of electrorheological elastomer sandwich beams, *Smart Mater. Struct.*, 2011, 20, 055012

[26] N. Tangboriboon, A. Sirivat and S. Wongkasemjit, Electrorheology and characterization of acrylic rubber and lead titanate composite materials, *Appl. Organometal. Chem.*, 2008, 22, 262-269

[27] L. Hao, C. Ding, X. Zhao, A novel electric elastomer based on starch/transformer oil drop/silicone rubber hybrid, *J. Appl. Polym. Sci.*, 2011, 119, 2991-2995

[28] L. Hao, Z. Shi and X. Zhao, mechanical behaviour of starch/silicone oil/silicone rubber hybrid electric elastomer, *Reactive & functional polymers*, 2009, 69, 165-169

[29] T. Puvanatvattana et Al., Electric field induced stress moduli in polythiophene/polyisoprene elastomer blends, *Reactive & functional polymers*, 2006, 66, 1575-1588

[30] N. Tangboriboon et Al., Electrorheological properties of novel piezoelectric lead zirconate titanate $Pb(Zr_{0.5},Ti_{0.5})O_3$-acrylic rubber composites, *Materials Science and engineering C,* 2009, 29, 1913-1918

[31] K. Thongsak et al.,Electroactive polydiphenylamine/poly(styrene-block-isoprene-block-styrene) (SIS) blends: Effects of particle concentration and electric field, *Materials Science and engineering C*, 2011, 31, 206-214

[32] R. Kunanuruksapong, A. Sirivat, Poly(p-phenylene) and acrylic elastomer blends for electroactive application, *Materials Science and engineering A*, 2007, 454-455, 453-460

[33] W. Kunchornsup, A. Sirivat, Physically cross-linked cellulosic gel via 1-butyl-3-methelimidazolium chloride ionic liquid and its electromechanical responses, *Sensors and actuators A*, 2012, 175, 155-164

[34] Seungae Lee, Chang-Min Yoon, Jin-Yong Hong and Jyongsik Jang, Enhanced electrorheological performance of a graphene oxide-wrapped silica rod with a high aspect ratio, *J. Mater. Chem. C*, 2014, 2, 6010-6016

[35] Sang Deuk Kim, Wen ling Zhang and Hyoung Jin Choi, Pickering emulsion-fabricated polystyrene-graphene oxide microspheres and their electrorheology, *J. Mater. Chem. C*, 2014, 2, 7541-7546

[36] Jinghua Wu, Ting Jin, Fenghua Liu, Jianjun Guo, Ping Cui, Yuchuan Cheng and Gaojie Xu, Preeparation of rod-like calcium titanyl oxalate with enhanced electrorheological activity and their morphological effect, *J. Mater. Chem. C*, 2014, 2, 5629-5635

[37] Y. Dong, Y. Liu, J. Yin and X. Zhao, Preparation and enhanced electro-responsive characteristic of graphene/layered double-hydroxide composite dielectric nanoplates, *J. Mater. Chem. C*, 2014, 2, 10386-10394

[38] Jian B. Yin and Xiao P. Zhao, Preparation and Electrorheological Activity of Mesoporous Rare-Earth-Doped TiO_2, *Chem. Mater*., 2002, 14 (11), 4633–4640

[39] Xiao P. Zhao and Jian B. Yin, Preparation and Electrorheological Characteristics of Rare-Earth-Doped TiO_2 Suspensions, *Chem. Mater*., 2002, 14 (5), 2258–2263

[40] Weijia Wen, Xianxiang Huang, Shihe Yang, Kunquan Lu & Ping Sheng, The giant electrorheological effect in suspensions of nanoparticles, *Nature Materials*, 2003, 2, 727 - 730

[41] Ying Dan Liu and Hyoung Jin Choi, Electrorheological fluids: smart soft matter and characteristics, *Soft Matter*, 2012, 8, 11961-11978

[42] A. Kossi, J. Persello and B. Cabane, Acetylacetone stimulus effect on electrorheological properties of TiO_2 aggregated nanoparticles, *J. Mater. Sci*., 2014, 49, 811-818

[43] H. Tang et al., Giant electrorheological effects of aluminium-doped TiO_2 nanoparticles, *Particuology*, 2010, 8, 442-446